Biosensors and Bioelectronics 202 (2022) 113991

Contents lists available at ScienceDirect

Biosensors and Bioelectronics

journal homepage: www.elsevier.com/locate/bios

Separation-free bacterial identification in arbitrary media via deep neural network-based SERS analysis

Eojin Rho [a,1], Minjoon Kim [b,1], Seunghee H. Cho [b], Bongjae Choi [a], Hyungjoon Park [b], Hanhwi Jang [b], Yeon Sik Jung [b,**], Sungho Jo [a,*]

[a] School of Computing, Korea Advanced Institute of Science and Technology (KAIST), Daejeon, 34141, Republic of Korea
[b] Department of Materials Science and Engineering, Korea Advanced Institute of Science and Technology (KAIST), Daejeon, 34141, Republic of Korea

ARTICLE INFO

Keywords:
Surface-enhanced Raman spectroscopy
Bacterial detection
Deep learning
E. coli
S. epidermidis

ABSTRACT

Universal and fast bacterial detection technology is imperative for food safety analyses and diagnosis of infectious diseases. Although surface-enhanced Raman spectroscopy (SERS) has recently emerged as a powerful solution for detecting diverse microorganisms, its widespread application has been hampered by strong signals from surrounding media that overwhelm target signals and require time-consuming and tedious bacterial separation steps. By using SERS analysis boosted with a newly proposed deep learning model named dual-branch wide-kernel network (DualWKNet), a markedly simpler, faster, and effective route to classify signals of two common bacteria *E. coli* and *S. epidermidis* and their resident media without any separation procedures is demonstrated. With outstanding classification accuracies up to 98%, the synergistic combination of SERS and deep learning serves as an effective platform for "separation-free" detection of bacteria in arbitrary media with short data acquisition times and small amounts of training data.

1. Introduction

Bacteria-induced illnesses, whether they are caused by direct bacterial infection or by exposure to bacterial toxins, can induce painful symptoms and even lead to death (Henkel et al., 2010). Therefore, rapid detection of bacteria is crucial to prevent the intake of contaminated foods and to diagnose infections from clinical samples, such as urine (Lazcka et al., 2007). However, conventional cultivation and plating methods can take days for accurate diagnoses, and more recent methods such as polymerase chain reaction or enzyme-linked immunosorbent assay have limited practicability as they also require laborious extraction and incubation steps that take at least several hours (Delehanty and Ligler, 2002; Jo et al., 2017; Yang et al., 2018).

As an alternative, surface-enhanced Raman spectroscopy (SERS) is an effective tool for the rapid acquisition of characteristic bacteria spectra. Molecule-specific spectra are obtained, where peaks at certain wavenumbers represent specific vibrations of molecular bonds (Schmidt et al., 2012). Past studies have successfully demonstrated the attainment of "fingerprint" Raman spectra of various bacteria, where spectral information from bacterial cell walls is obtained by placing cells on noble metal nanostructures that significantly enhance inherently weak Raman signals (Wang et al., 2016). Among the various media used for bacterial dispersion, water is frequently chosen because it has a sufficiently small Raman cross section and provides minimum signal interference for relatively easy attainment of water-dispersed bacteria spectra (Sengupta et al., 2006; Zhou et al., 2014). Nevertheless, because there are many overlapping peak sources such as proteins in cell walls, it is often challenging to obtain consistent and clear spectra (Lorenz et al., 2017; Witkowska et al., 2019). Consequently, it may be difficult to distinguish signals from different bacterial types by simply identifying their key peaks, and therefore statistical methods such as principal component analysis (PCA) have been applied for spectral classification (Wang et al., 2016).

Furthermore, direct detection of bacteria in solutions (e.g., broth medium) is more challenging because bacterial signals are substantially overlapped by those from the media itself or are masked by an additional fluorescence background that leads to noisy spectra (Butler et al., 2016; Marotta and Bottomley, 2010; Yang et al., 2018). In recent research, to

* Corresponding author.
** Corresponding author.
E-mail addresses: ysjung@kaist.ac.kr (Y.S. Jung), shjo@kaist.ac.kr (S. Jo).
[1] These authors contributed equally to this work.

https://doi.org/10.1016/j.bios.2022.113991
Received 10 June 2021; Received in revised form 4 January 2022; Accepted 7 January 2022
Available online 18 January 2022

reduce solution interference, bacteria have been extracted from their media in ways such as membrane filtration after antibody and nanoparticle attachment or selective capturing of bacteria cells onto a functionalized nanostructured surface (Cho et al., 2015; Liu et al., 2011). However, bacteria separation steps are usually tedious and thus require additional preparation time, which takes much longer than needed for Raman measurements and subsequent analysis procedures (Yang et al., 2018). Therefore, a more effective approach that can overcome the medium signal-interference issues and provide much-improved cost-effectiveness and measurement throughput is needed.

In this study, we developed an original approach to rapidly identify bacterial signals measured directly in various media by implementing a highly accurate newly developed deep learning model, Dual-Branch Wide Kernel Network (DualWKNet). Deep learning is a state-of-the-art artificial intelligence method for hierarchical extraction of features using multiple layers with trainable parameters and has been applied to various fields including computer vision and natural language processing (Goodfellow et al., 2016; He et al., 2016; Vaswani et al., 2017) It has also been applied to Raman spectroscopy with models such as a 1D convolution neural network architecture adapted from the ResNet model (1D-ResNet) (Ho et al., 2019) and a deep learning-based component identification (DeepCID) model proposed to determine the chemical components of a mixture via analysis of their Raman spectra (Fan et al., 2019). In contrast to these previous models that simply modified 2D image analysis models from computer vision research, we designed the DualWKNet model that efficiently learns the correlation between spectral features that are important in analyzing 1D spectral data. The DualWKNet model consists of two separate branches of large kernel sizes to extract and learn features in spectral data. As a result, while previous deep learning-based SERS analysis required thousands of data per class to correctly learn and distinguish spectra (Fan et al., 2019; Ho et al., 2019), DualWKNet showed excellent performance with few hundred spectra that requires significantly less data collection time.

To the best of our knowledge, this is the first study to combine SERS and deep learning to collect and distinguish SERS signals of bacteria in multiple media, without laborious bacteria separation or capturing procedures. The Raman signals of *E. coli* and *S. epidermidis* dispersed in water, artificial urine, ground beef solution, milk, and nutrient broth were obtained by placing samples on SERS substrates and collecting Raman data. Then, the data collected from each medium was categorized into three classes, two bacteria types and the medium, by using the DualWKNet model that was trained with the attained data. We achieved up to 98% accuracy in categorizing bacterial spectra with five-fold cross-validation tests. Through this strategy, we demonstrate that bacterial signals can be distinguished from those of the medium to show that they can be identified despite the existence of highly interfering media signals. Ultimately, this deep learning-based SERS analysis method for bacterial identification shows great promise as a rapid detection and diagnostic tool that can be extended to classify more diverse bacteria and solution types.

2. Materials and methods

2.1. Bacteria sample preparation

Escherichia coli (*E. coli* NEB E4104S) and *Staphylococcus epidermidis* (*S. epidermidis* KCTC 1917) were obtained from New England Biolabs and the Korean Collection for Type Cultures, respectively. Bacteria were stored in mixtures of glycerol and broth solutions prior to growth for Raman measurements. For sample preparation, 0.5 mL of each mixture was added to 50 mL of each respective broth solution for overnight incubation at 37 °C. A sample of each mixture (1 mL) was then transferred to new fresh broth solutions (50 mL) and incubated at 37 °C for a further 4 h for *E. coli* and 7 h for *S. epidermidis*.

To harvest bacteria cells, the solutions were centrifuged once to separate the cells from the broth solutions and centrifuged an additional two times in deionized water to wash off the remnants of the broth solutions (Premasiri et al., 2011). Subsequently, the cells were mixed with solutions of the five chosen media (i.e., water, artificial urine, ground beef solution, milk, and nutrient broth) and diluted to $OD_{600} = 0.4$. Deionized water was used as the water medium, and artificial urine produced by Pickering Laboratories was used as the urine medium. Ground beef solution was prepared by dispersing 2 g of ground beef in 20 mL of deionized water and filtered through syringe filters having pore sizes of 0.45 μm (Cho et al., 2015). Milk and nutrient broth media were prepared by diluting 1 mL of sterilized milk and nutrient broth solution each in deionized water to reduce solution viscosity and to more easily identify bacterial cells with Raman optical microscopy. Before Raman measurements, 5 μL of a bacteria-containing solution or the medium solution was dropped and dried on Ag-based SERS substrates purchased from Silmeco. SEM images of the SERS substrates were taken with a field-emission SEM (Hitachi S-4800; Supplementary Fig. 1).

2.2. Raman spectra collection

Raman spectra were measured using a dispersive Raman spectrometer (ARAMIS, Horiba Jobin Yvon). A 514 nm Ar-ion laser with a power of 0.3 mW and a diameter of 1 μm was focused on the sample for 0.5 s per spectrum acquisition with a Raman shift range of 500–2000 cm^{-1}. A × 100 microscope and gratings with 1200 grooves per 1 mm were used. Assuming that the center of a cell would have maximized contact area with the substrate for best signal enhancement, the laser spot was aimed at the center of a bacterial cell. To perform five-fold cross-validation tests, 500 spectra of each class of *E. coli*, *S. epidermidis*, and residing medium were collected. For comparison with a focus on spectral features, all spectra were normalized after removing major fluorescence backgrounds. Baseline correction was carried out on each spectrum using the iterative polynomial fitting method of 100 iterations with a fitting order of five (Liland et al., 2010).

2.3. Deep learning architecture adaptation and training

For accurate discrimination of bacteria and their residing media, we developed the DualWKNet model to analyze the obtained Raman spectra. The model comprises a dual-branch network, wherein a single network branch includes residual blocks and average pooling layers, followed by a self-attention block. The residual blocks in each branch have different kernel sizes, acting as filters that extract and learn various spectral features. The use of a multi branch network and a self-attention block was adapted from the multi-stream self-attention model (Han et al., 2019), which exhibits excellent performance in speech recognition capabilities. Additional details concerning the implementation of the model are provided in Supplementary Note 1 and in the Results and discussion section.

To distinguish the spectra of *E. coli*, *S. epidermidis*, and the residing medium, DualWKNet returned probabilities for the three classes during both training and testing. The class having the highest probability was selected as the predicted class. DualWKNNet was written in Python language and utilized the Pytorch deep learning framework (Paszke et al., 2019). The model training was performed using the Titan V (NVIDIA, USA) GPU.

2.4. Attributing the prediction of deep learning model

We used the integrated gradient method to explain which input features contributed to our model's class prediction (Sundararajan et al., 2017). The integrated gradient indicates how much the input $x \in \mathbb{R}^n$ contributes to the predictions relative to the baseline, $x' \in \mathbb{R}^n$, when there is a deep learning model represented by the function, $F : \mathbb{R}^n \rightarrow [0, 1]$. When $\frac{\partial F(x)}{\partial x_i}$ is a gradient of $F(x)$ along the i^{th} dimension, the integrated gradient can be approximated with Equation (1).

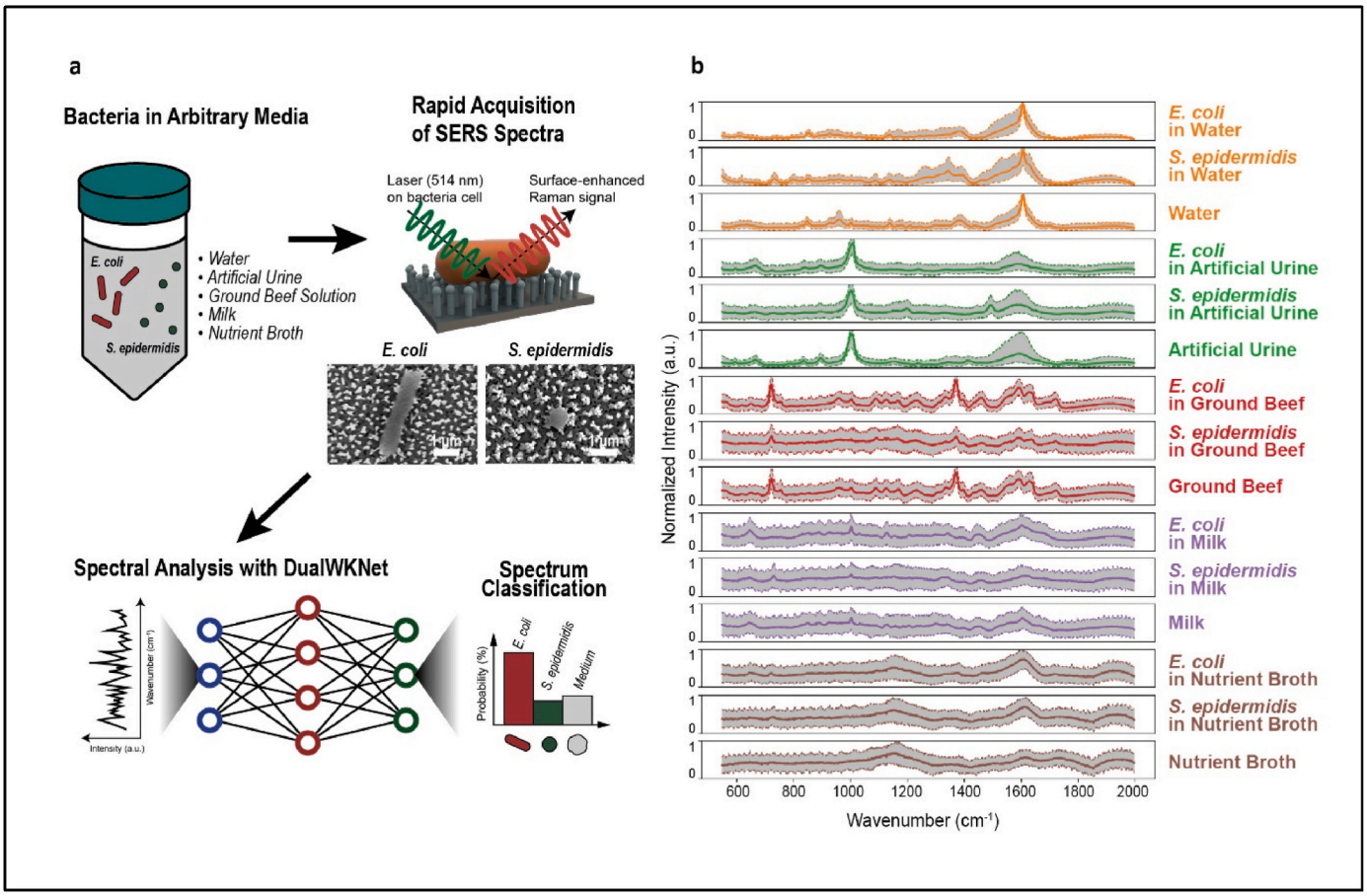

Fig. 1. General experimental procedure with analyte images and measured Raman spectra. (a) Schematics of the general process of Raman data collection and analysis where a single spectrum is attained from a single cell and classified via deep learning. (b) Average Raman spectra for each class from 5th to 95th percentiles after background removal. 500 spectra were processed and averaged for each class.

$$\text{IntegratedGrads}_i(x) \approx \left(x_i - x_i^{'}\right) \times \Sigma_{k=1}^{m} \frac{\partial F\left(x^{'} + \frac{k}{m} \times (x - x^{'})\right)}{\partial x_i} \times \frac{1}{m}. \quad (1)$$

3. Results and discussion

3.1. Bacteria spectra collection and limitations of PCA analysis

Escherichia coli (*E. coli* NEB E4104S) and *Staphylococcus epidermidis* (*S. epidermidis* KCTC 1917) were selected as the target bacteria to demonstrate the detection of representative gram-negative and positive bacteria, respectively. Each bacterium was grown in its respective optimal broth solution and dispersed into different testing media solutions where the two bacterial types have been reported to be identified. Artificial urine was selected as a medium to detect the two bacteria as indicators of urinary tract infections (Cegelski et al., 2008; Kloβ et al., 2013), and nutrient broth solution was chosen as a common growth medium (Jonas et al., 2018; Saito et al., 2019). Water, ground beef solution, and milk were selected for food safety analyses (Cho et al., 2015; Fan et al., 2011; Jaglic et al., 2010; Li et al., 2018; Sin et al., 2014; Zhou et al., 2014). Samples for Raman data collection were prepared by dropping and drying 5 μL of bacteria-containing solutions ($OD_{600} = 0.4$) onto commercial Ag-based SERS substrates consisting of dense Ag-coated nanopillar arrays with excellent Raman enhancement and uniformity (Fig. 1a, Supplementary Fig. 1; Schmidt et al., 2012; Wu et al., 2017).

Spectra of individual cells and their detection media were each collected 500 times with short acquisition times of 0.5 s. To prevent cell damage and graphitization that lead to spectra consisting mostly of graphitic peaks, the laser-filter values were optimized so that the laser intensities were not too strong, successfully producing Raman peaks that were eligible for class identification (Efrima and Zeiri, 2009). The average spectra are shown in the average plot in Fig. 1b, where the boundary lines represent the intervals for 5th to 95th percentiles. Here, it can be observed that the general shapes of the spectra for each class in a medium appeared similar. The medium contributes to the overall Raman signal by providing overlapping signals and fluorescence that may be due to concentrations or Raman cross sections that are larger than those of cells (Butler et al., 2016; Marotta and Bottomley, 2010; Yang et al., 2018). Therefore, individual spectra from each class can be difficult to differentiate by identifying clear peaks, and PCA was carried out to examine the statistical distribution of the data based on their principal components (Supplementary Fig. 2). Additionally, the average signal-to-noise ratio (SNR) in each medium was calculated to support the distribution of the data points, because it is generally more facile to differentiate spectra with high SNR values (Supplementary Table 1). Accordingly, data measured in water and artificial urine had high SNR values greater than 10 and were more separated from other classes in the PCA plots. By contrast, the Raman data measured for ground beef solution, milk, and nutrient broth had low SNR values below 4 and overlapped to greater extents, reflecting the limitations of classification using PCA. These observations suggest that advanced classification methods are required for more accurate results.

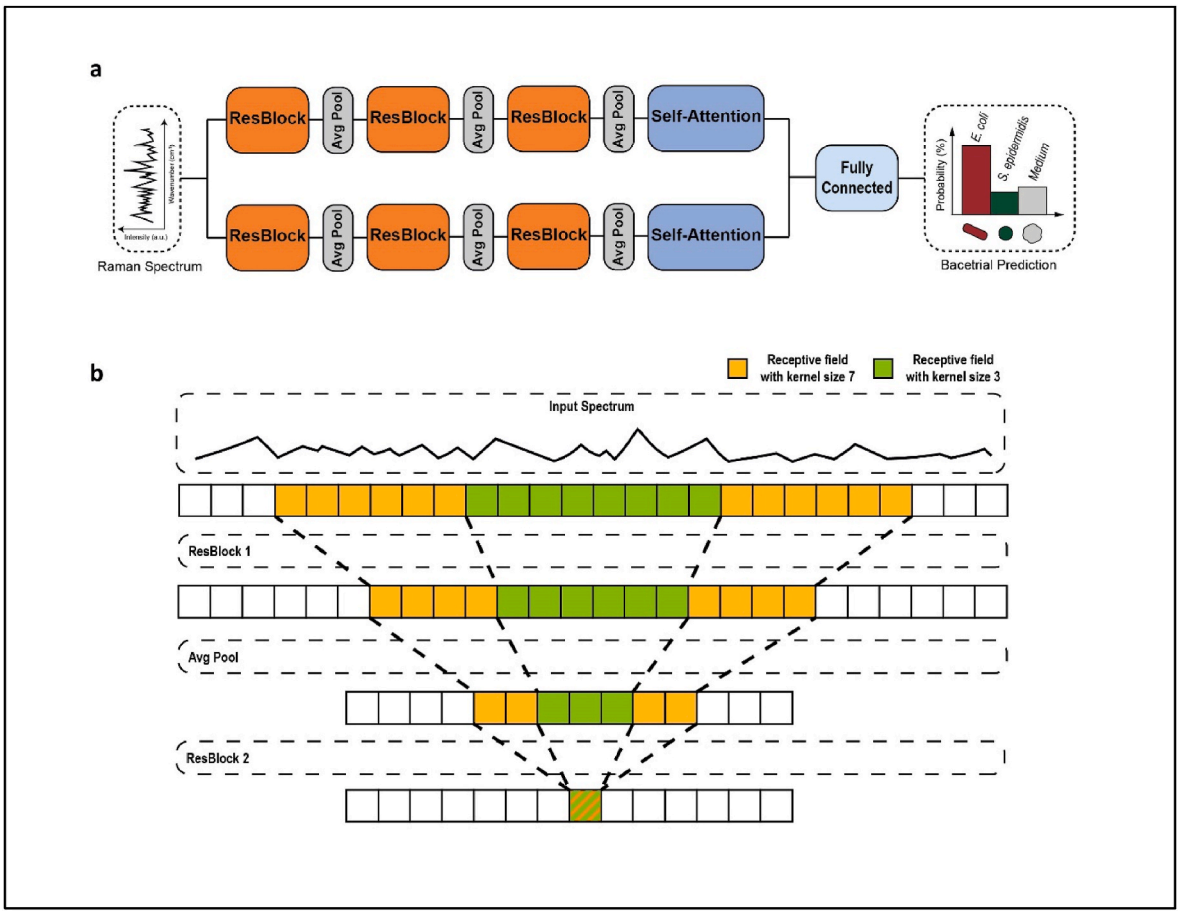

Fig. 2. Configuration of the DualWKNet model. (a) Dual branch network where residual blocks extract spectral features and subsequent self-attention blocks learn the relations between spectral features. The final fully connected layer returns the probability of each bacterial class. (b) Simplified diagram of the DualWKNet model up to the second residual block to show the difference in receptive field area with differing kernel sizes. Each block represents a data point in a given Raman spectrum. The orange colored-area represents an example case with a kernel size of 7 while the green colored-area represents the case with a kernel size of 3. The orange regions cover larger areas due to a larger kernel size.

3.2. DualWKNet deep learning model

The proposed DualWKNet model comprises two separate network branches (Fig. 2a). Each network branch has three sets of residual blocks and average pooling layers, followed by a self-attention block. The residual block serves as a filter that extracts spectral features from a given input while the pooling layer reduces the number of spectral features and learning parameters and prevents overfitting. This differs from the 1D ResNet model that uses residual blocks without a pooling layer and the DeepCID model that uses a max-pooling layer instead of an average pooling layer. Max pooling layers use maximum values of features in the filter window that lead to information loss, and average pooling layers are applied in DualWKNet to use average values that minimize information loss and increase the overall classification accuracy (Supplementary Table 2). The self-attention block then finds the correlation between spectral features to further identify important information so that the final fully-connected layer can return the probability of each class (*E. coli*, *S. epidermidis*, and residing media) for classification.

Importantly, the DualWKNet model has a dual network so that the residual blocks of each network branch have different kernel sizes that allow the network branches to extract and learn different spectral features. A residual block includes a convolution layer as a trainable filter, and the kernel size of the convolution layer can be viewed as the filter size. The optimal kernel size for analyzing Raman spectra measured in each residing media can vary, and a single branch network with fixed kernel sizes shows lower performance than the dual branch network because the kernel sizes may not be ideal for data measured in certain media (Results in Supplementary Fig. 3 and configurations in Supplementary Fig. 4). However, a multi-branch network with more than two branches may result in overfitting because it has too many trainable parameters. Thus, our model was designed by configuring dual branch networks of appropriately different kernel sizes to maintain high classification performance for various media.

The DualWKNet model also has large kernel sizes, or wide kernels, for accurate training of global features with few training data. Previous convolution neural network-based models learn global features of data by applying deep networks consisting of numerous convolution blocks to have large receptive fields that prevent the omission crucial information during analysis of spectral data (Luo et al., 2016). However, overfitting can occur with such deep networks with few training data, which leads to loss in classification accuracies (Supplementary Fig. 5). As a solution, our model was constructed to have shallow networks with three sets of residual bocks that have large kernel sizes (>15) in contrast to previous models that used small kernel sizes (three to five). This prevents overfitting and allows our model to have large receptive fields despite having fewer number of convolution layers. The representation in Fig. 2b shows that with larger receptive fields due to larger kernel sizes, more spectral features, or global features, can be considered for the analysis of important features for each class.

Table 1
Comparison of the five-fold classification accuracies of DualWKNet, DeepCID, 1D-ResNet, and classical machine-learning techniques in identifying the two bacteria and their media.

		Accuracies (%) for Classification of *E. coli*, *S. epidermidis*, and Media				
		Water	**Artificial Urine**	**Ground Beef Solution**	**Milk**	**Nutrient Broth**
Machine Learning	3-NN	87.7 ± 1.4	82.1 ± 1.5	59.2 ± 1.0	56.5 ± 3.3	64.7 ± 2.6
	PCA-SVM	93.9 ± 1.6	91.7 ± 1.3	83.6 ± 1.7	82.1 ± 2.4	79.9 ± 2.0
	LR	94.5 ± 1.0	93.8 ± 1.2	83.1 ± 1.9	81.1 ± 0.5	80.1 ± 1.6
Deep Learning	1D-ResNet	97.2 ± 1.3	93.1 ± 1.5	82.5 ± 2.3	79.0 ± 2.4	76.3 ± 1.4
	DeepCID	96.8 ± 1.3	94.0 ± 1.1	83.7 ± 1.4	79.7 ± 1.0	80.0 ± 1.8
Our Model	DualWKNet	**98.0 ± 0.8**	**96.6 ± 1.1**	**88.3 ± 1.7**	**86.4 ± 0.9**	**84.3 ± 2.0**

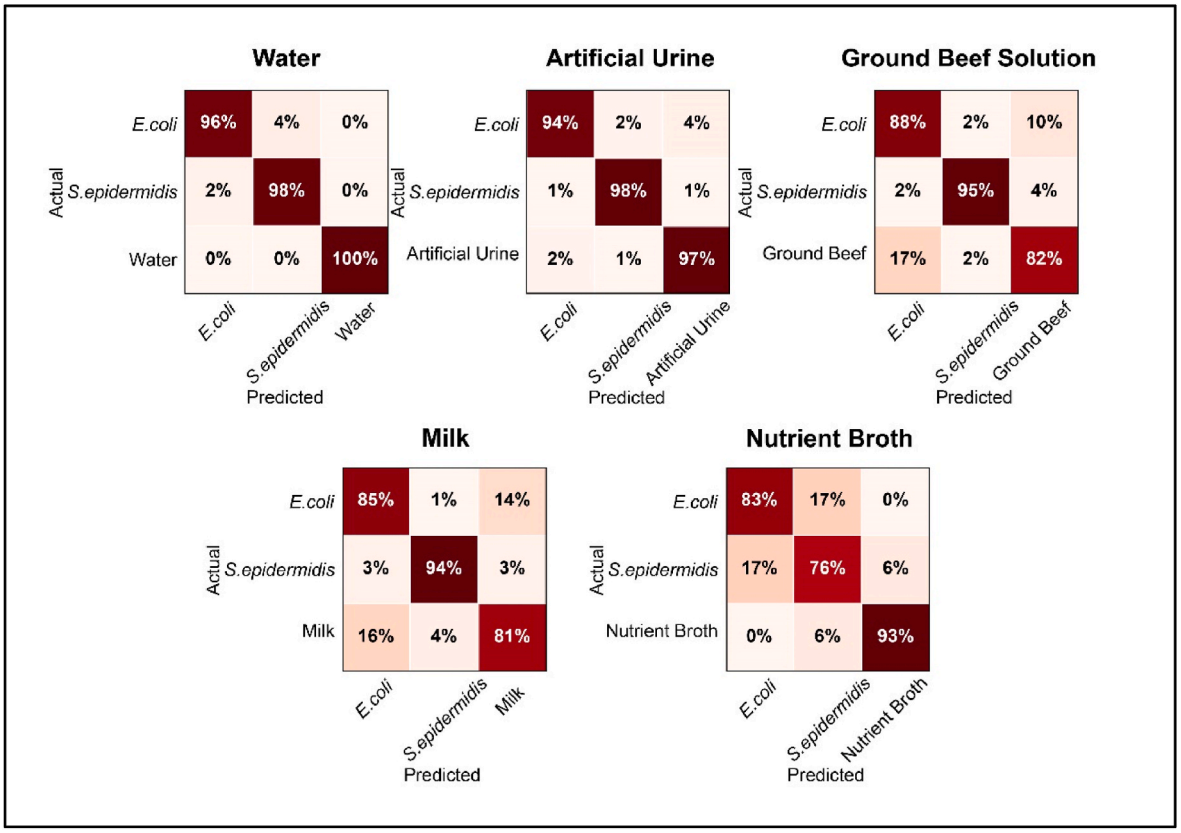

Fig. 3. Confusion matrices representing the identification accuracy for each class of the proposed model. Each confusion matrix shows the classification accuracy of *E. coli*, *S. epidermidis*, and the residing media. The row represents the actual class, whereas the column represents the class predicted by the proposed model. Each entry in the confusion matrix was measured using five-fold cross-validation and is a percentage out of 500 bacteria.

3.3. Five-fold classification results

The DualWKNet model then successfully performs the classification task of Raman spectra of two bacteria (i.e., *E. coli* and *S. epidermidis*) in five different residing media (i.e., water, artificial urine, ground beef solution, milk, and nutrient broth) (Table 1). We conducted five-fold cross-validation tests to measure the classification accuracy of different learning models. The 500 spectra of each bacteria and medium class were divided into five random groups of equal data size. Each group in turn was used for classification, while the remaining data were used for training the learning model. The DualWKNet model demonstrated the best classification performance in all residing media, compared with classical machine learning models (3-nearest neighbor (3-NN), support vector machine with PCA (PCA-SVM), and logistic regression (LR)) as well as previous deep learning models (i.e., 1D ResNet and DeepCID). Here, the classification performance in different media varied and was related to the calculated SNR values (Supplementary Table 1). The data measured in water and artificial urine had high average SNR values of 22.8 and 11.2, which led to excellent accuracies of 98.0 and 96.6%, respectively, with the DualWKNet model. However, owing to the lower average SNR values above 3.0 in ground beef solution, milk, and nutrient broth, the classification performances in these media were measured to be below 90% at 88.3, 86.4, and 84.3%, respectively. Nevertheless, while the ResNet and DeepCID models produced no significant increases in identification accuracies compared with classical machine learning techniques in such noisy data, the DualWKNet model displayed accuracies of at least 3% or higher than all other techniques.

For additional examination of the identification accuracy in each medium, confusion matrices were constructed (Fig. 3). The identification accuracies (i.e., true positive rates) are shown in the red diagonal sections and correlate to the classification results of distinct media. The accuracy values exceeded 90% for those measured in water and artificial urine, whereas the average values of bacterial discrimination were approximately 90% in ground beef solution and milk. In nutrient broth, although the accuracies for separate bacteria identification were 83% or

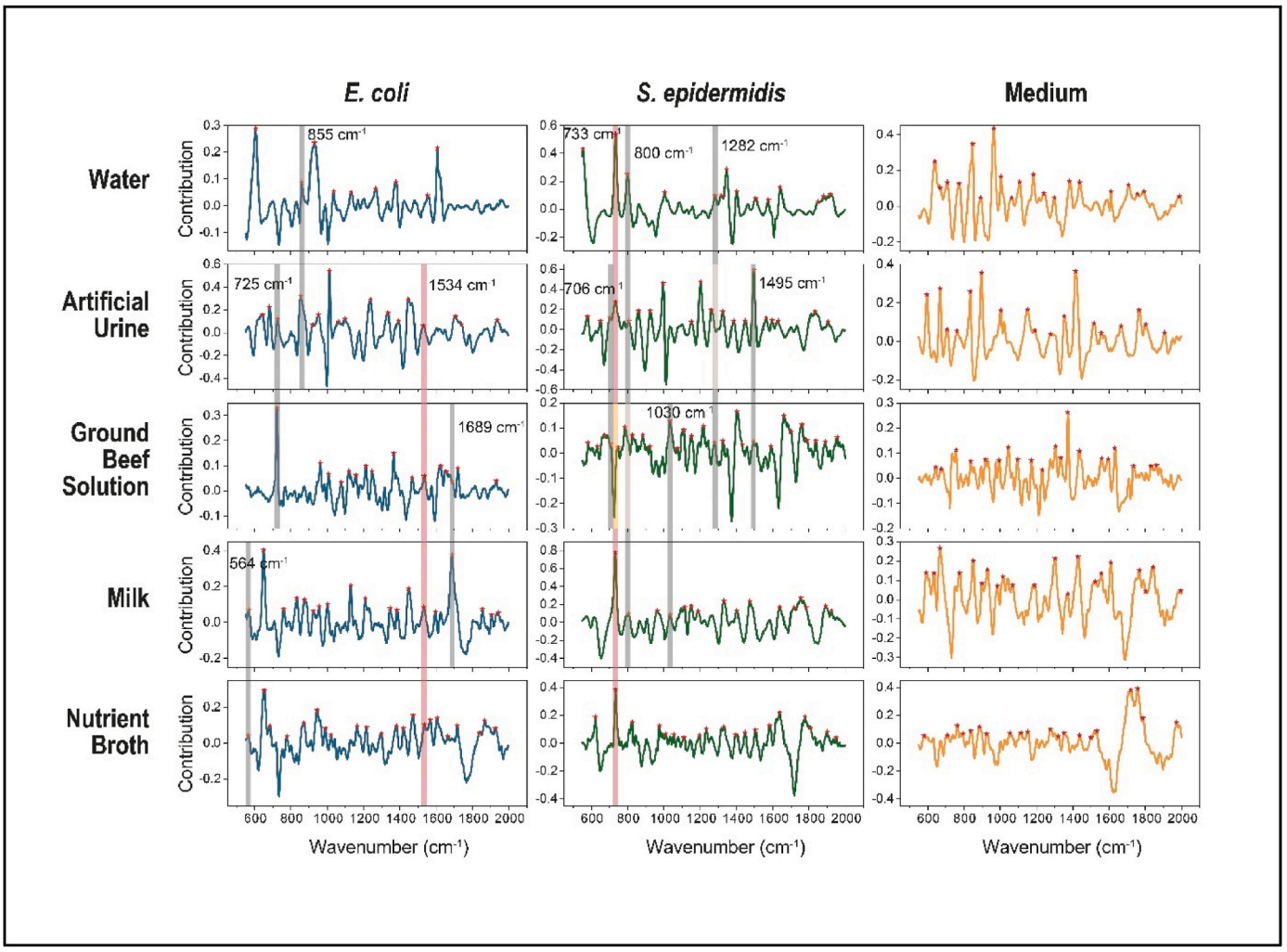

Fig. 4. Average contribution spectra of each class in separate media. Classes measured in the same medium are arranged in rows, whereas the classes of same bacteria are arranged in columns. Peaks of a bacterium that are identical in up to four media are marked with pink bars. Other identical peaks are shown with grey bars.

below, it was highly unlikely to misclassify bacteria as the pure medium itself with misclassification rates of 0% for *E. coli* and 6% for *S. epidermidis*.

3.4. Factors in identification of bacteria

To examine the features for distinguishing different bacteria and their respective media, the contribution percentage for class identification was determined at each wavenumber using the integrated gradient method (Sundararajan et al., 2017). As shown in Fig. 4, the average contribution spectra for the true positive spectra of the confusion matrices in Fig. 3 are plotted. True positive spectra are selected because they constitute most of the dataset in each class and can be used to analyze the truly contributing peaks for identification. As previously noted in Fig. 1, the general spectrum shapes of the two bacteria are similar to that of the medium, thus making the classification of individual spectra challenging. The DualWKNet model significantly enhances the classification accuracy by identifying different key peaks, many of which are almost indiscernible in individual spectra (peak positions are noted in Supplementary Table 3), for reference during differentiation. Therefore, in contrast to the average Raman spectra, the average contribution spectra of each bacteria in a medium appeared less similar because of their different peak positions in addition to varying contribution percentages, which is the basis for discrimination of noisy or similar-looking spectra.

The contribution peaks are crucial for distinguishing different classes of a single medium, but the contribution peaks of a single bacterial type may not be identical in varying media. As shown in Fig. 4 and Supplementary Table 3, the number of identified contributing peaks varied in each medium, and the peak positions were partially identical. For example, the maximum number of mediums showing specific similar peak positions was four near 1534 cm^{-1} (assigned to hypoxanthine) in *E. coli* spectra and 733 cm^{-1} (derived from adenine) in *S. epidermidis* spectra (Fan et al., 2011; Yang et al., 2018). For the 733 cm^{-1} peak of S. *epidermidis*, it was not identified as a contributing peak in ground beef solution, but it was observed in the average Raman spectrum. As shown in Fig. 1b, the ground beef solution medium exhibited a peak at a similar position that overlapped with the bacterium signal and was not considered to be a significant contribution point for the bacterium in the respective medium. Thus, it was not essential for the same bacterium to have identical contributing peaks in all media. With numerous signal sources in a cell that overlap with medium signals with varying amounts of noise or diverse peak positions, different peaks may be more important or identifiable in various media.

4. Conclusions

This paper presents highly effective and rapid separation-free

identification of *E. coli* and *S. epidermidis* in various residing media by analyzing their SERS spectra with the novel DualWKNet deep learning model. By using a dual-branch network with different and wide kernel sizes, an optimal design for classification in multiple media was achieved to successfully identify common contribution peaks for classification. Despite having interfering signals or noise from the media as well as limited amounts of training data, high classification accuracies up to 98% were achieved with five-fold cross-validation tests. Overall, our approach provides a meaningful universal platform for potential biomedical applications and can be extended to examine more bacterial types as well as other media that are important for food or clinical analysis, such as blood.

CRediT authorship contribution statement

Eojin Rho: Conceptualization, Software, Formal analysis, Writing – original draft. **Minjoon Kim:** Conceptualization, Methodology, Investigation, Writing – original draft. **Seunghee H. Cho:** Methodology, Writing – review & editing. **Bongjae Choi:** Formal analysis, Writing – review & editing. **Hyungjoon Park:** Methodology, Writing – review & editing. **Hanhwi Jang:** Investigation. **Yeon Sik Jung:** Conceptualization, Supervision, Project administration. **Sungho Jo:** Conceptualization, Supervision, Project administration.

Declaration of competing interest

The authors declare that they have no known competing financial interests or personal relationships that could have appeared to influence the work reported in this paper.

Acknowledgments

This work was supported by the National R&D Program through the National Research Foundation of Korea (NRF) grant (2022M3H4A1A01012816) funded by the Ministry of Science and ICT (MSIT).

Appendix A. Supplementary data

Supplementary data to this article can be found online at https://doi.org/10.1016/j.bios.2022.113991.

References

Butler, H.J., Ashton, L., Bird, B., Cinque, G., Curtis, K., Dorney, J., Esmonde-White, K., Fullwood, N.J., Gardner, B., Martin-Hirsch, P.L., Walsh, M.J., McAinsh, M.R., Stone, N., Martin, F.L., 2016. Nat. Protoc. 11 (4), 664–687.
Cegelski, L., Marshall, G.R., Eldridge, G.R., Hultgren, S.J., 2008. Nat. Rev. Microbiol. 6 (1), 17–27.
Cho, I.-H., Bhandari, P., Patel, P., Irudayaraj, J., 2015. Biosens. Bioelectron. 64, 171–176.
Delehanty, J.B., Ligler, F.S., 2002. Anal. Chem. 74 (21), 5681–5687.
Efrima, S., Zeiri, L., 2009. J. Raman Spectrosc. 40 (3), 277–288.
Fan, C., Hu, Z., Mustapha, A., Lin, M., 2011. Appl. Microbiol. Biotechnol. 92 (5), 1053–1061.
Fan, X., Ming, W., Zeng, H., Zhang, Z., Lu, H., 2019. Analyst 144 (5), 1789–1798.
Goodfellow, I., Bengio, Y., Courville, A., 2016. Deep Learning. MIT Press.
Han, K.J., Prieto, R., Ma, T., 2019. State-of-the-art speech recognition using multi-stream self-attention with dilated 1d convolutions. In: 2019 IEEE Automatic Speech Recognition and Understanding Workshop (ASRU). IEEE, pp. 54–61.
He, K., Zhang, X., Ren, S., Sun, J., 2016. Deep residual learning for image recognition. In: Proceedings of the IEEE Conference on Computer Vision and Pattern Recognition. IEEE Computer Society, Las Vegas, NV, USA, pp. 770–778.
Henkel, J.S., Baldwin, M.R., Barbieri, J.T., 2010. EXS 100, pp. 1–29.
Ho, C.-S., Jean, N., Hogan, C.A., Blackmon, L., Jeffrey, S.S., Holodniy, M., Banaei, N., Saleh, A.A., Ermon, S., Dionne, J., 2019. Nat. Commun. 10 (1), 1–8.
Jaglic, Z., Michu, E., Holasova, M., Vlkova, H., Babak, V., Kolar, M., Bardon, J., Schlegelova, J., 2010. Epidemiol. Infect. 138 (5), 772–782.
Jo, Y., Park, S., Jung, J., Yoon, J., Joo, H., Kim, M.-h., Kang, S.-J., Choi, M.C., Lee, S.Y., Park, Y., 2017. Sci. Adv. 3 (8), e1700606.
Jonas, A.M., Glinel, K., Behrens, A., Anselmo, A.C., Langer, R.S., Jaklenec, A., 2018. ACS Appl. Mater. Interfaces 10 (19), 16250–16259.
Kloß, S., Kampe, B., Sachse, S., Rösch, P., Straube, E., Pfister, W., Kiehntopf, M., Popp, J., 2013. Anal. Chem. 85 (20), 9610–9616.
Lazcka, O., Campo, F.J.D., Muñoz, F.X., 2007. Biosens. Bioelectron. 22 (7), 1205–1217.
Li, L., Li, Q., Liao, Z., Sun, Y., Cheng, Q., Song, Y., Song, E., Tan, W., 2018. Anal. Chem. 90 (15), 9621–9628.
Liland, K.H., Almøy, T., Mevik, B.-H., 2010. Appl. Spectrosc. 64 (9), 1007–1016.
Liu, T.-Y., Tsai, K.-T., Wang, H.-H., Chen, Y., Chen, Y.-H., Chao, Y.-C., Chang, H.-H., Lin, C.-H., Wang, J.-K., Wang, Y.-L., 2011. Nat. Commun. 2 (1), 538.
Lorenz, B., Wichmann, C., Stöckel, S., Rösch, P., Popp, J., 2017. Trends Microbiol. 25 (5), 413–424.
Luo, W., Li, Y., Urtasun, R., Zemel, R., 2016. Understanding the effective receptive field in deep convolutional neural networks. Adv. Neural Inf. Process. Syst. 4898–4906.
Marotta, N.E., Bottomley, L.A., 2010. Appl. Spectrosc. 64 (6), 601–606.
Paszke, A., Gross, S., Massa, F., Lerer, A., Bradbury, J., Chanan, G., Killeen, T., Lin, Z., Gimelshein, N., Antiga, L., Desmaison, A., Kopf, A., Yang, E., DeVito, Z., Raison, M., Tejani, A., Chilamkurthy, S., Steiner, B., Fang, L., Bai, J., Chintala, S., 2019. PyTorch: an imperative style, high-performance deep learning library. In: Wallach, H., Larochelle, H., Beygelzimer, A., Alché-Buc, F., Fox, E., Garnett, R. (Eds.), Advances in Neural Information Processing Systems, 32. Curran Associates, Inc, pp. 8024–8035.
Premasiri, W.R., Gebregziabher, Y., Ziegler, L.D., 2011. Applied Spectroscopy 65 (5), 493–499.
Saito, M., Ishiki, K., Nguyen, D.Q., Shiigi, H., 2019. Anal. Chem. 91 (20), 12793–12798.
Schmidt, M.S., Hubner, J., Boisen, A., 2012. Adv. Mater. 24 (10), OP11–18.
Sengupta, A., Mujacic, M., Davis, E.J., 2006. Anal. Bioanal. Chem. 386 (5), 1379–1386.
Sin, M.-C., Sun, Y.-M., Chang, Y., 2014. ACS Appl. Mater. Interfaces 6 (2), 861–873.
Sundararajan, M., Taly, A., Yan, Q., 2017. Axiomatic attribution for deep networks. JMLR.org, Sydney, NSW, Australia, pp. 3319–3328.
Vaswani, A., Shazeer, N., Parmar, N., Uszkoreit, J., Jones, L., Gomez, A.N., Kaiser, Ł., Polosukhin, I., 2017. Attention is all you need. In: Proceedings of the 31st International Conference on Neural Information Processing Systems. Curran Associates Inc., Long Beach, California, USA, pp. 6000–6010.
Wang, P., Pang, S., Chen, J., McLandsborough, L., Nugen, S.R., Fan, M., He, L., 2016. Analyst 141 (4), 1356–1362.
Witkowska, E., Niciński, K., Korsak, D., Szymborski, T., Kamińska, A., 2019. Anal. Bioanal. Chem. 411 (10), 2001–2017.
Wu, K.Y., Rindzevicius, T., Schmidt, M.S., Thilsted, A.H., Boisen, A., 2017. J. Raman Spectrosc. 48 (12), 1808–1818.
Yang, D., Zhou, H., Dina, N.E., Haisch, C., 2018. R. Soc. Open Sci. 5 (9), 180955.
Zhou, H., Yang, D., Ivleva, N.P., Mircescu, N.E., Niessner, R., Haisch, C., 2014. Anal. Chem. 86 (3), 1525–1533.